This article has been accepted for publication in IEEE Communications Letters. This is the author's version which has not been fully edited and content may change prior to final publication. Citation information: DOI 10.1109/LCOMM.2024.3380741

RIS-Aided Wireless Fingerprinting Localization Based on Multilayer Graph Representations

Stefania Sardellitti, *Senior Member, IEEE,* Paolo Di Lorenzo, *Senior Member, IEEE,* and Sergio Barbarossa, *Fellow, IEEE*

***Abstract*—The aim of this paper is to propose a novel method for wireless fingerprinting localization empowered by reconfigurable intelligent surfaces (RISs), exploiting the flexibility offered by RIS configuration control, and coping with the possible lack of received signal strength information (RSSI) at certain locations. The proposed approach hinges on a graph-based radio map interpolation method, which encodes similarities between model-generated RSSI, collected across spatial and fingerprints domains through the topology of a multi-layer graph. Numerical results illustrate the advantages of the proposed approach with respect to previous methods, in terms of both radio map recovery and accuracy of wireless localization.**

***Index Terms*—Fingerprinting localization, reconfigurable intelligent surfaces, radio map recovery, graph signal processing.**

I. Introduction

In the last few years, RISs gained increasing popularity as a promising technology to realize dynamic transformations of the wireless propagation environment, in both indoor and outdoor scenarios [1], [2]. Reconfigurable Intelligent Surfaces (RISs) are identified as a crucial technology for 6G, enabling the formation of controllable reflected beams that dynamically establish service-enhanced areas. These areas can dynamically balance capacity, energy efficiency, localization accuracy, and reliability to meet the specific demands of the moment and location [3], [4]. As communications evolve towards millimeter-wave frequencies and beyond, RISs offer valuable alternatives for maintaining connectivity when direct links are blocked. Research has concentrated on enhancing RIS-empowered wireless communication and edge computing for this purpose [5]–[7]. Additionally, RISs are instrumental for high-precision wireless localization, enabling advancements in applications such as biomedical and security imaging, indoor mapping, and passive sensing. They also facilitate the integration of sensing, localization, communication, and computing, thereby bolstering security and trust in 6G networks through the strategic use of location data [4], [8].

An overview of the main opportunities and challenges associated with RIS-empowered wireless localization is provided in [9], while different localization strategies are proposed in [8], [10]–[15]. Specifically, the authors in [10] present a user localization method aided by multiple RISs with an initial step for direction estimation at each RIS, followed by maximum likelihood position estimation. In [8] the authors proposed a multiple RSSI fingerprint based localization scheme in RIS-assisted systems, where the optimal RIS configurations are derived and employed for location estimation using deep neural networks. In [11] a general signal model valid for near- and far-field localization is proposed, while in [12] the authors investigated supervised learning feature selection methods to prune the large state space of the RIS and enhance localization accuracy. In [13] the authors analysed a method based on the Fisher information to optimize the RIS phases in order to improve localization performance. The effect of signal degradation on RIS-aided localization due to non-linearities in hardware is examined in [14]. Finally, the work in [15] proposed a RIS-aided fingerprinting localization method that leverages projected gradient descent for the selection of RIS configurations and neural networks for location estimation.

In this paper, following the approach proposed in [8], [15], we focus on wireless fingerprinting localization (WFL) empowered by RISs. In this approach, the flexibility of RISs is exploited to create a set of signal fingerprints (one for each RIS configuration), which is then compared to the ones contained into pre-stored radio maps for localization purposes. This avoids the need of having a large set of known anchors, such as base stations (BSs) or access points, to create a sufficient number of fingerprints for user localization, thus reducing the overall cost of the system. However, differently from [8], [15], we do not assume to have access to the full radio maps, which is typically a costly and time consuming process, as it requires to perform many measurements at different locations. Instead, only a sub-sampling of measurements in the radio maps is available, calling for the development of suitable data augmentation methods enabling any WFL algorithm. To this aim, several interpolation methods have been proposed in the literature such as, e.g., inverse distance weighting [16], radial basis functions [17], neural networks [18], graph-based interpolation [19]. Our approach is similar to the one used in [19], since we also exploit graph signal processing (GSP) tools to interpolate radio maps. However, differently from [19], we explicitly take RISs into account in both the construction and the interpolation of the radio maps. More specifically, exploiting a set of spatially coherent beams controllable via the RISs, we model the RSSI measurements as *signals defined over a multi-layer graph* that encodes data similarities across both the spatial and the fingerprints domains. Then, this versatile model enables us to exploit GSP tools to recover the observed radio maps from a limited number of samples. Finally, the inferred radio maps are exploited for RIS-aided wireless fingerprinting localization. Our approach extends the one proposed in [19] in terms of considered scenario and system modeling, offering a higher level of flexibility during sampling and, consequently, a large improvement in terms of radio map interpolation and user localization. Numerical

This work has been supported by the EU H2020 RISE-6G project under grant number 101017011. The authors are with the Department of Information Engineering, Electronic and Telecommunications (DIET), Sapienza University of Rome, Rome, Italy. E-mail:{stefania.sardellitti, paolo.dilorenzo, sergio.barbarossa}@uniroma1.it.

Authorized licensed use limited to: Universita degli Studi di Roma La Sapienza. Downloaded on May 07,2024 at 07:34:19 UTC from IEEE Xplore. Restrictions apply.
© 2024 IEEE. Personal use is permitted, but republication/redistribution requires IEEE permission. See https://www.ieee.org/publications/rights/index.html for more information.

This article has been accepted for publication in IEEE Communications Letters. This is the author's version which has not been fully edited and content may change prior to final publication. Citation information: DOI 10.1109/LCOMM.2024.3380741

results illustrate the advantage of the proposed approach with respect to other methods available in the literature, in terms of radio map estimation precision and user localization accuracy.

II. Background

A. Graph Signal Processing Tools

Let us consider an undirected graph $\mathcal{G} = \{\mathcal{V}, \mathcal{E}\}$ where $\mathcal{V} = \{1, \dots, N\}$ is the set of N nodes and $\mathcal{E} = \{a_{ij}\}_{i,j\in\mathcal{V}}$ denotes the edge set with $a_{ij} > 0$, if there is a link between node i and node j, or $a_{ij} = 0$, otherwise. The connectivity relations among the nodes of the graph $\mathcal{G}$ are captured by the adjacency matrix $\mathbf{A} = \{a_{ij}\}_{i,j=1}^{N} \in \mathbb{R}^{N\times N}$, which collects all the edge weights a_{ij} for $i, j = 1, \dots, N$. The combinatorial graph Laplacian is defined as $\mathbf{L} \triangleq \mathbf{K} - \mathbf{A}$, where $\mathbf{K}$ is the degree diagonal matrix containing the node degrees $d_i = \sum_j a_{ij}$ for $i = 1, \dots, N$ on its diagonal. This matrix is symmetric and positive semidefinite for undirected graphs and admits the eigendecomposition $\mathbf{L} = \mathbf{U}\mathbf{\Lambda}\mathbf{U}^T$, where $\mathbf{U}$ is the matrix with columns the eigenvectors $\{\boldsymbol{u}_i\}_{i=1}^{N}$ of $\mathbf{L}$, and $\mathbf{\Lambda}$ is a diagonal matrix containing the eigenvalues of $\mathbf{L}$.

A signal $\mathbf{x}$ over a graph $\mathcal{G}$ is defined as a mapping from the vertex set to the set of real numbers, i.e., $\mathbf{x} : \mathcal{V} \to \mathbb{R}$. For undirected graphs, the Graph Fourier Transform (GFT) $\hat{\mathbf{x}}$ of a graph signal $\mathbf{x}$ is defined as the projection of $\mathbf{x}$ onto the subspace spanned by the eigenvectors $\mathbf{U} = \{\boldsymbol{u}_i\}_{i=1}^{N}$ of the Laplacian matrix $\mathbf{L}$, i.e., $\hat{\mathbf{x}} = \mathbf{U}^T\mathbf{x}$ [20]. An $\mathcal{F}$-bandlimited graph signal can then be represented as $\mathbf{x} = \mathbf{U}_{\mathcal{F}}\hat{\mathbf{x}}_{\mathcal{F}}$, where $\mathbf{U}_{\mathcal{F}} = \{\boldsymbol{u}_i\}_{i\in\mathcal{F}}$ denotes the collection of Laplacian eigenvectors over the frequency indexes $\mathcal{F}$, and $\hat{\mathbf{x}}_{\mathcal{F}}$ are the related (graph) Fourier coefficients. If a graph signal is bandlimited, graph sampling theory enables the recovery of the overall signal from observations collected over a subset $\mathcal{S}$ of nodes, with $|\mathcal{S}| < N$ [20]. In particular, let $\mathbf{z} = \mathbf{D}_{\mathcal{S}}\mathbf{x}$ be the sampled signal, with $\mathbf{D}_{\mathcal{S}}$ denoting the node-selection diagonal matrix (whose i-th diagonal entry is 1 if $i \in \mathcal{S}$, and 0 otherwise). Then, starting from the sampled signal $\mathbf{z}$, we can recover $\mathbf{x}$ via the interpolation formula [20]

$$\mathbf{x} = \mathbf{U}_{\mathcal{F}}\left(\mathbf{U}_{\mathcal{F}}^T\mathbf{D}_{\mathcal{S}}\mathbf{U}_{\mathcal{F}}\right)^{-1}\mathbf{U}_{\mathcal{F}}^T\mathbf{z}, \tag{1}$$

provided that the (necessary and sufficient) condition $\mathrm{rank}(\mathbf{D}_{\mathcal{S}}\mathbf{U}_{\mathcal{F}}) = \mathrm{rank}(\mathbf{U}_{\mathcal{F}}) = |\mathcal{F}|$ is satisfied, which strongly depends on the selected set of graph samples $\mathcal{S}$ [20].

B. RIS-aided Channel Model

Let us consider a 2D scenario, with a single-antenna BS located at $\mathbf{p}_{tx} \in \mathbb{R}^2$ and K RISs centered at $\mathbf{p}_{RIS_k} \in \mathbb{R}^2$, $k = 1, \dots, K$. Each RIS is modeled as an M-element uniform linear array with spacing $\lambda/2$, denoting by λ the signal wavelength. The receiving UE, equipped with single antenna, has (unknown) location $\mathbf{p} \in \mathbb{R}^2$. The discrete-time signal received at the UE consists of a line-of-sight (LoS) component plus K reflected signals from RISs according to [13]:

$$y = \left(\sum_{k=1}^{K} \alpha_k \mathbf{h}_k^T \mathbf{\Phi}_k \mathbf{g}_k + \alpha_d h_d\right) s + n \tag{2}$$

where $\mathbf{h}_k \in \mathbb{C}^{M\times 1}$ denotes the channel vector between the k-RIS and the UE, $\mathbf{\Phi}_k$=diag$(\phi_{1,k}, \dots, \phi_{M,k})$ is an $M \times M$ diagonal matrix accounting for the phase shifts applied by the M elements of the RIS k, with $\phi_{n,k} = e^{j\omega_{n,k}}$, $n = 1, \dots, M$; $\mathbf{g}_k \in \mathbb{C}^{M\times 1}$ is the BS to RIS k channel vector, while $s = \sqrt{P_s}\,\zeta$ is the transmitted signal with power P_s, and ζ denotes the unit-power complex information symbol chosen from a discrete constellation set. Finally, h_d is the channel coefficient of the LoS link from the BS to the UE, and $n \sim \mathcal{CN}(0, \sigma_n^2)$ represents the Gaussian additive noise at the receiver. The path loss coefficients α_d and $\{\alpha_k\}_{k=1}^{K}$ are modeled, with respect to a location centered in $\mathbf{p}$, as $\alpha_d = e^{-j2\pi f_c \tau_d}\frac{\lambda\alpha_{sd}}{4\pi\|\mathbf{p}-\mathbf{p}_{tx}\|}$ and $\alpha_k = e^{-j2\pi f_c \tau_k}\frac{\lambda^2\alpha_{sk}}{16\pi^2\|\mathbf{p}_{RIS_k}-\mathbf{p}_{tx}\|\|\mathbf{p}-\mathbf{p}_{RIS_k}\|}$, where f_c is the carrier frequency, α_{sd}, α_{sk} are attenuation coefficients accounting for the shadowing effects by physical obstacles, and we define the time delays as $\tau_d = \|\mathbf{p} - \mathbf{p}_{tx}\|/c$, $\tau_k = \|\mathbf{p}_{RIS_k} - \mathbf{p}_{tx}\|/c + \|\mathbf{p} - \mathbf{p}_{RIS_k}\|/c$, with c denoting the speed of light [13], [14]. According to (2), the BS-RIS$_k$ and RIS$_k$-UE channel vectors are modeled as $g_{m,k} = \exp(j\pi m \sin(\theta_k))$ and $h_{m,k} = \exp(j\pi m \sin(\gamma_k))$, for $m = 0, \dots, M-1$, where θ_k is the angle of arrival (AoA) of the signal from BS to RIS$_k$, and γ_k is the angle of departure (AoD) of the signal from the RIS$_k$ to the UE. The RSSI measured by the UE at position $\mathbf{p}$ is given by $r = |y|^2$, with y given in (2).

III. Multi-layer Graph Signal Model for RIS-aided Wireless Fingerprints

Let us consider the RIS-aided wireless scenario in Sec. II.B. Since we are interested in RIS-aided WFL [8], [15], we assume that UEs can measure only the RSSI at their given location, and the RISs employ different configurations (i.e., different phase shifts $\{\mathbf{\Phi}_k\}_{k=1}^{K}$ in (2)) to generate multiple and diverse fingerprints. Then, we partition the area of interest according to a regular grid composed of N nodes, where each point represents a candidate user location. For a given BS and RIS configuration l, we denote by $\mathbf{r}^l \in \mathbb{R}^N$ the vector composed of the RSSI measurements (i.e., fingerprints) collected over the grid, whose i-th entry represents the RSSI observed at node i. An RSSI signal field, composed of L different fingerprint vectors $\{\mathbf{r}^l\}_{l=1}^{L}$, is collected to enable WFL [8], [15]. The RSSI signal field is defined by two domains, i.e., a spatial domain reflecting the propagation environment, and a fingerprint domain generated by the multiple RISs configurations.

In this paper, we propose to model the set of fingerprints $\{\mathbf{r}^l\}_{l=1}^{L}$ generated by L different RIS configurations as signals defined over a multi-layer graph, which encodes the dependencies between the space and fingerprint domains. To be more specific, we consider a multilayer graph $\overline{\mathcal{G}}$ with L graph layers $\mathcal{G}^l = \{\mathcal{V}, \mathcal{E}^l\}$, $l = 1, \dots, L$, each consisting of a common vertex set $\mathcal{V}$, placed over the spatial grid of UEs locations, and a set $\mathcal{E}^l$ of intra-layer edges. Then, the overall multi-layer graph $\overline{\mathcal{G}} = \{\overline{\mathcal{V}}, \overline{\mathcal{E}}\}$ has a set of vertices $\overline{\mathcal{V}}$ composed of $N_L = NL$ nodes, and an edge set $\overline{\mathcal{E}} = \mathcal{E}_I \cup \mathcal{E}_B$, where $\mathcal{E}_I = \cup_{l=1}^{L}\mathcal{E}^l$ and $\mathcal{E}_B$ are the sets connecting nodes inside and between layers, respectively. A pictorial example is given in Fig. 1, where we show three radio maps generated by three different RIS configurations in a scenario with $K = 2$ RISs and one BS. The gray areas represent obstacles and the environment is discretized over a (spatial) grid composed by

Authorized licensed use limited to: Universita degli Studi di Roma La Sapienza. Downloaded on May 07,2024 at 07:34:19 UTC from IEEE Xplore. Restrictions apply.
© 2024 IEEE. Personal use is permitted, but republication/redistribution requires IEEE permission. See https://www.ieee.org/publications/rights/index.html for more information.

This article has been accepted for publication in IEEE Communications Letters. This is the author's version which has not been fully edited and content may change prior to final publication. Citation information: DOI 10.1109/LCOMM.2024.3380741

$N = 53$ nodes. The connectivity pattern in Fig. 1 represents the multi-layer graph encoding both intra- and inter-layer similarities between spatial points at different fingerprints.

Let us now define the $N_L \times N_L$-dimensional multilayer adjacency matrix $\overline{\mathbf{A}}$. Given the multi-layer nature of the graph, the adjacency $\overline{\mathbf{A}} = \{\mathbf{A}_{lm}\}_{l,m=1}^{L}$ is a block matrix, where each diagonal block $\mathbf{A}_{ll} \in \mathbb{R}^{N\times N}$ encodes the connectivity of layer l (i.e., spatial correlations), for $l = 1, \ldots, L$, and each off-diagonal block $\mathbf{A}_{lm} \in \mathbb{R}^{N\times N}$ describes connections between layers l and m (i.e., correlations in the fingerprint domain), for all $l, m = 1, \ldots, L$ with $l \neq m$. The structure of the multi-layer graph adjacency might be learnt if RSSI information is available at each point of the grid. However, in this paper, we assume that only partial RSSI information is available over both the spatial and fingerprint domains. To cope with such lack of data, we exploit a model-based approach for the multi-layer graph construction. In particular, we generate synthetic RSSI values $\{\bar{\mathbf{r}}^l\}_{l=1}^{L}$ according to the signal model in (2). Then, we adopt the following criterion to connect node i with node j intra- and across-layers:

$$A_{lm}(i,j) = \begin{cases} w_{lm}(i,j) & \text{if } \mid \bar{\boldsymbol{r}}^l(i) - \bar{\boldsymbol{r}}^m(j) \mid \leq \epsilon, \\ 0 & \text{o.w,} \end{cases} \tag{3}$$

for all $i, j = 1, \ldots, N$ and $l, m = 1, \ldots, L$, where ϵ is a fixed threshold and $w_{lm}(i,j)$ are the link weights that can be chosen as functions of the physical distance between the nodes or of the correlation of signals observed over them. This approach enables to build a similarity (multi-layer) graph based on the model in (2), which can be specifically tuned to the scenario at hand. Clearly, true RSSI measurements will suffer from model mismatching, whose effect will be assessed via numerical simulations in Sec. V. Finally, once defined the adjacency $\overline{\mathbf{A}}$, we can introduce the $N_L \times N_L$ Laplacian matrix associated with the multi-layer graph as $\overline{\mathbf{L}} = \overline{\mathbf{K}} - \overline{\mathbf{A}}$.

IV. Graph-based Radio Map Interpolation and Fingerprinting Localization

In this section, we exploit the multi-layer graph signal model presented in Sec. III to perform radio map interpolation from a limited collection of RSSI measurements over space and fingerprint domains. To this aim, we hinge on the GSP tools introduced in Sec. II.A and, in particular, on the interpolation formula in (1). To apply (1), given the (eigenvectors of) Laplacian matrix $\overline{\mathbf{L}}$, we need to select two sets: i) the signal bandwidth $\mathcal{F}$, i.e., the set of frequency indexes used for signal interpolation; ii) the sampling set $\mathcal{S}$ where to observe RSSI values. To select a suitable bandwidth $\mathcal{F}$, we resort again on the synthetic RSSI values $\bar{\mathbf{r}} = \{\bar{\mathbf{r}}^l\}_{l=1}^{L}$ obtained via the signal model in (2). In particular, we look for the sparsest representation of the vector $\bar{\mathbf{r}} = [\bar{\mathbf{r}}^1; \ldots; \bar{\mathbf{r}}^L]$ over the basis composed by the (multi-layer) Laplacian eigenvectors, say $\overline{\mathbf{U}}$, solving the convex basis pursuit problem [21]:

$$\begin{aligned} \min_{\hat{\mathbf{r}} \in \mathbb{R}^{N_L}} \quad & \| \hat{\mathbf{r}} \|_1 \\ \text{s.t.} \quad & \| \bar{\mathbf{r}} - \overline{\mathbf{U}} \hat{\mathbf{r}} \|_F \leq \beta \end{aligned} \tag{4}$$

where the l_1-norm forces sparsity on the entries of $\hat{\boldsymbol{r}}$, while the constraint keeps the representation error lower than a prescribed accuracy according to the threshold $\beta > 0$. The rational is to find the representation of signal $\hat{\boldsymbol{r}}$ that is more compact (i.e., bandlimited) in the graph frequency domain. Then, the set of non-zero elements (i.e., the support) of the solution $\hat{\boldsymbol{r}}$ of problem (4) is used as bandwidth $\mathcal{F}$.

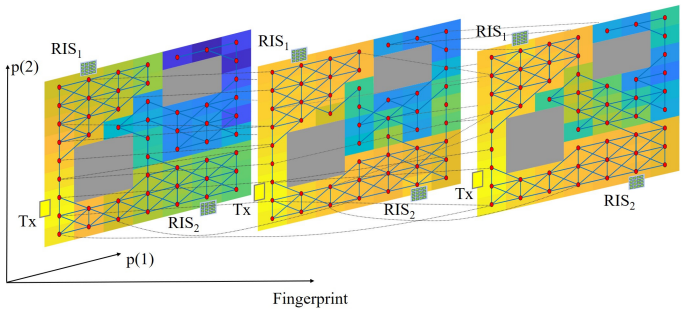

Fig. 1. Example of multilayer graph encoding spatial-fingerprint relations.

Once the bandwidth $\mathcal{F}$ is decided, we have to choose a suitable sampling set $\mathcal{S}$ enabling stable graph signal recovery. To this aim, we exploit one of the several methods available in the GSP literature, see, e.g., [20] and references therein. Interestingly, the sampling strategy applied to our multi-graph representation gives information about which data (over spatial and fingerprint domains) are more important to collect in order to recover the overall signal field from a limited number of observations. This feature represents a useful planning tool for telcom operators interested in practical implementation of RIS-aided WFL. Finally, assuming to have collected a set of (real) RSSI measurements $\mathbf{z} = \mathbf{D}_{\mathcal{S}}\mathbf{r}$ over the sampling set $\mathcal{S}$, the overall radio maps vector $\mathbf{r} = [\mathbf{r}^1; \ldots; \mathbf{r}^L]$ can be (approximately) recovered applying (1) as

$$\tilde{\mathbf{r}} = \overline{\mathbf{U}}_{\mathcal{F}} \left(\overline{\mathbf{U}}_{\mathcal{F}}^T \mathbf{D}_{\mathcal{S}} \overline{\mathbf{U}}_{\mathcal{F}} \right)^{-1} \overline{\mathbf{U}}_{\mathcal{F}}^T \mathbf{z}. \tag{5}$$

Fingerprinting localization. The recovered maps can finally be used by the network operator for WFL. Specifically, let us denote by $\mathbf{m} = [m_1, \ldots, m_L]^T \in \mathbb{R}^{L\times 1}$ the set of RSSI measurements collected by the UE at some unknown position $\mathbf{p}$. The vector $\mathbf{m}$ is then compared with the recovered maps $\tilde{\mathbf{r}} = \{\tilde{\mathbf{r}}^l\}_{l=1}^{L} \in \mathbb{R}^{NL}$, which are conveniently reshaped in matrix form as $\tilde{\mathbf{R}} = [\tilde{\mathbf{r}}^1, \ldots, \tilde{\mathbf{r}}^L]^T \in \mathbb{R}^{L\times N}$. To estimate the UE position, several criteria can be adopted, as for example a minimum distance (MD) or a maximum correlation coefficient (MC) criterion [12]. Then, denoting by $\tilde{\mathbf{R}}_{l,\bullet}$ the l-th column of matrix $\tilde{\mathbf{R}}$, the MD method returns the optimal position $l^\star$ (over the grid) of the UE such that it holds

$$l^\star = \arg \min_{l \in \{1,\ldots,N\}} d(l) = \|\tilde{\mathbf{R}}_{l,\bullet} - \mathbf{m}\|, \tag{6}$$

while the MC criterion takes a decision for the UE position $l^\star$ according to the following rule:

$$l^\star = \arg \max_{l \in \{1,\ldots,N\}} \rho(l) = \frac{\tilde{\mathbf{R}}_{l,\bullet}^T \mathbf{m}}{\|\tilde{\mathbf{R}}_{l,\bullet}\| \|\mathbf{m}\|}. \tag{7}$$

To improve localization accuracy we can also apply a k-nearest neighbour (k-NN) method hinging on the MD and MC strategies. Specifically, the coefficients $d_p(l)$ and $\rho(l)$ are

Authorized licensed use limited to: Universita degli Studi di Roma La Sapienza. Downloaded on May 07,2024 at 07:34:19 UTC from IEEE Xplore. Restrictions apply.
© 2024 IEEE. Personal use is permitted, but republication/redistribution requires IEEE permission. See https://www.ieee.org/publications/rights/index.html for more information.

This article has been accepted for publication in IEEE Communications Letters. This is the author's version which has not been fully edited and content may change prior to final publication. Citation information: DOI 10.1109/LCOMM.2024.3380741

Algorithm 1 : RIS-Aided Wireless Fingerprinting Localization based on Multilayer Graph Representations

Input: $\mathbf{p}_{tx}$, λ, f_c, M, P_s, ϵ; $\mathbf{p}_{RIS_k}$, $\mathbf{h}_k$, $\mathbf{g}_k$, for all $k = 1,\dots,K$; $\mathbf{\Phi}_k^l$ for all $k = 1,\dots,K$, $l = 1,\dots,L$.
(S1) Generate L synthetic RSSI measurements $\bar{\mathbf{r}} = \{\bar{\mathbf{r}}^l\}_{l=1}^L$ via the signal model in (2);
(S2) Build the multilayer graph adjacency according to (3);
(S3) Find the graph signal bandwidth $\mathcal{F}$ solving (4);
(S4) Select the multilayer sampling set $\mathcal{S}$ according to a graph sampling criterion available in the literature [20];
(S5) Recover the radio maps $\tilde{\mathbf{r}}$ according to (5);
(S6) Perform user localization using (6) or (7);
Output: Radio maps $\tilde{\boldsymbol{r}}$ and UEs position estimates.

sorted in increasing and decreasing order, respectively, and for each strategy the estimated UE location is computed as the average of the locations corresponding to the first k nodes.

Overall algorithm. To summarize, the proposed multi-layer graph-based learning and localization strategy consists of three main operations: 1) Learn the multi-layer graph exploiting the RIS-aided channel model; 2) Apply GSP tools to find sparse graph signal representations, identify the sampled nodes where the RSSI measurements are observed, and interpolate the radio maps; 3) Apply RIS-aided WFL using the recovered radio maps. For the sake of clarity of exposition, we list all the steps of the proposed method in Algorithm 1.

Remark on complexity. The complexity of Algorithm 1 is mainly driven by step (S3), which requires the computation of the eigenvector matrix $\overline{\mathbf{U}} \in \mathbb{R}^{NL\times NL}$ and its usage in (4). To reduce complexity in the case of large-scale graphs, we propose to split the observed frame of fingerprints in N_f independent blocks, each composed of L_C fingerprints with high degree of correlation. This can be achieved by generating spatially correlated fingerprints through L_C different RIS configurations. In this way, the multilayer graph in the fingerprints domain is split into N_f disconnected multilayer graphs, each composed of L_C layers, thus largely reducing the overall complexity of Laplacian eigenvector computation.

V. Numerical results

In this section, we evaluate the performance of our approach in both radio map interpolation and user localization. We consider an area of 20×10 m^2, with one BS placed at $(0, 2)$, and two RISs placed at $(5, 10)$ and $(15, 0)$, respectively. At the center of the scenario, we place an obstacle of area 20×10 m^2, which introduces an additive attenuation of 50dB in the received signal. Each RIS is modeled as a uniform linear array with $M = 25$ elements spaced by $\lambda/2$. The area is discretized using a grid of $N = 150$ points, placed at a distance of 1 m. The BS works at 1 GHz with power $P_s = 5$dBW.

Radio map interpolation. We generate $N_f L_C = 100$ fingerprints configurations with $L_C = 4$ so that the observed frame is split in $N_f = 25$ multilayer graphs each composed of $L = 4$ layers. To generate RIS fingerprints, we consider the phase shifts $\omega_{n,k} = \pi(n-1)\sin(\bar{\omega}_k)$, for each element n of the RIS k, and we randomly vary the phase shifts $\bar{\omega}_k$ between $(0, \pi)$.To recover the radio maps strategy, we first learn the multi-layer graph from the model-generated signals using (3) with $\epsilon = 4$ (step (S2) of Algorithm 1). We assume in our experiments w.l.o.g. binary link weights. Then, we solve problem (4) for several values of β, i.e. for different signal estimation error (step (S3)). The resulting sparse signal representation are used to recover the overall map from a limited number of RSSI measurements applying the formula in (5) and by using the D-optimal design criterion [20] to find the sampled set $\mathcal{S}$ (steps (S4)-(S5)). The goodness of the radio map interpolation is illustrated in Fig. 2, where we report the normalized mean squared error (NMSE) averaged over 100 radio maps, versus the (average) number N_s of samples per layer. To illustrate the advantage of our approach with respect to a simpler graph-based model, in Fig. 2 we downgrade our interpolation method to the case when only spatial relations among points are considered (i.e., neglecting relationships among fingerprints). In this case, the graphs associated with the different radio maps are independent on each other. To make a fair comparison, we select the same number of samples N_s per layer for the two approaches. For the graph-based approach, we select the largest bandwidth enabling reconstruction (i.e., N_s), selecting the (spatial) Laplacian eigenvectors through (4). As we can see from Fig. 2, the multi-layer graph representation provides a remarkable gain in terms of estimation performance. This gain is due to our joint approach, which models multiple radio maps as a single graph signal defined over a multi-layer graph, incorporating similarities over both spatial and fingerprint domains. In this way, the selection of samples and bandwidth is done over the entire multi-layer graph, thus giving a higher level of flexibility during sampling and, consequently, a large improvement in terms of interpolation.

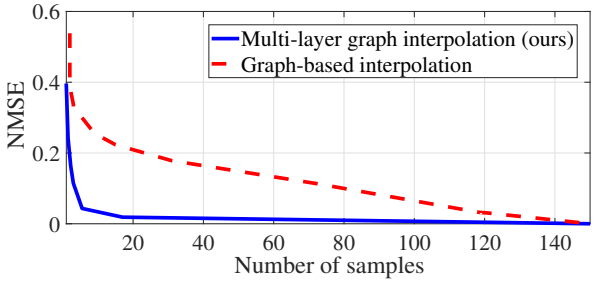

Fig. 2. NMSE versus the number of observed samples, for different methods.

Mobile user localization. Let us consider the same scenario as before, where mobile users are randomly placed within the area of interest. Then, we apply Algorithm 1 to perform radio map interpolation and user localization, using D-optimal sampling [20] and a k-NN method based on MD criterion with $k = 4$ neighbors. To account for possible model mismatching between reality and the RIS-aided channel model in Sec. II.B, the recovered maps are corrupted with Gaussian noise with zero-mean and standard deviation σ. Then, in Fig. 3, we illustrate the localization error $\|\hat{\mathbf{p}} - \mathbf{p}\|$, averaged over 300 random user positions and over 100 noise realizations, versus the number of RIS configurations used in the localization phase, considering different noise standard deviations σ. From Fig. 3, as expected, we notice how the localization error diminishes increasing the number of RIS configurations;

Authorized licensed use limited to: Universita degli Studi di Roma La Sapienza. Downloaded on May 07,2024 at 07:34:19 UTC from IEEE Xplore. Restrictions apply.
© 2024 IEEE. Personal use is permitted, but republication/redistribution requires IEEE permission. See https://www.ieee.org/publications/rights/index.html for more information.

This article has been accepted for publication in IEEE Communications Letters. This is the author's version which has not been fully edited and content may change prior to final publication. Citation information: DOI 10.1109/LCOMM.2024.3380741

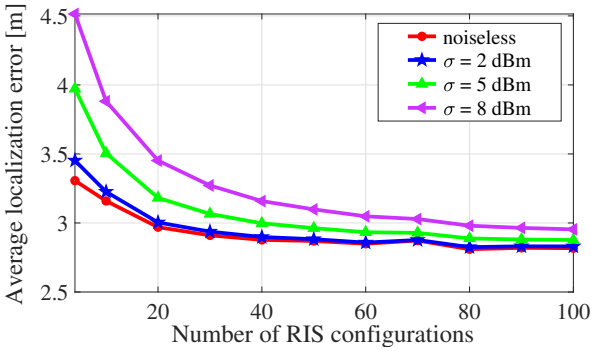

Fig. 3. Localization error vs RIS configurations, for different noise conditions.

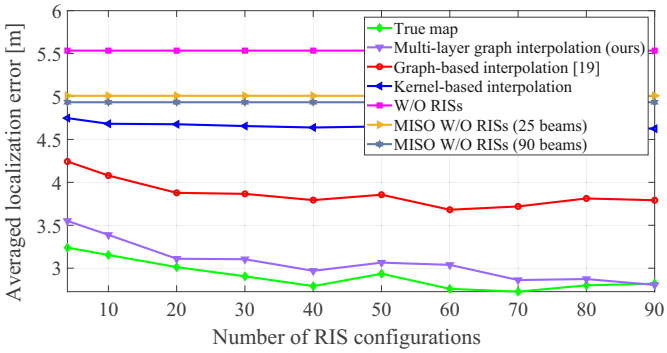

Fig. 4. Localization error vs. RIS configurations, for different strategies.

also, we can notice the robustness of our method to model mismatching. Finally, in Fig. 4, we compare the localization performance of our method with respect to other approaches: i) a graph-based interpolation strategy (e.g., the one in [19] generalized to our scenario); ii) a (Gaussian) kernel-based signal interpolation method; iii) two benchmarks named "True map" and "W/O RISs", representing the case of full knowledge of radio maps and absence of RISs, respectively; iv) a graph-based interpolation without RISs, with BS having $N_t = 25$ antennas ("MISO W/O RISs"). For all the methods, the average number of samples over each graph (i.e., layer) is equal to 20. From Fig. 4, we can notice how the proposed approach exhibits considerable performance gain compared with both the graph-based method in [19] and the kernel-based interpolation approach, getting performance very close to the optimal benchmark (i.e., "True map"). The enhancement in localization accuracy is achieved thanks to improved radio map estimation capability of the proposed multi-layer graph representation. Finally, our method also outperforms the worst benchmark where the system does not leverage the presence of RISs. This improvement holds also in the MISO case, as the use of multiple antennas at the BS cannot mitigate signal blockage caused by physical obstacles, even using a large number of different beams (e.g., 25 or 90 in Fig. 4).

VI. Conclusions

In this paper we introduced a novel topology-driven strategy for the recovery of radio maps to be used in RIS-aided wireless fingerprinting localization. The approach hinges on multi-layer graphs that capture and exploit the spatial-fingerprints correlations among the RSSI signals in a joint fashion. Exploiting graph signal processing tools, this novel representation enables efficient recovery of radio maps from a limited number of observed samples, thus enhancing the overall localization performance. Several research directions are open, including the incorporation of more realistic and complex (e.g., MIMO) RIS-aided channel models, and methods to learn the multi-layer graph topology that maximizes the localization accuracy.

References

[1] M. Di Renzo *et al.*, "Smart radio environments empowered by reconfigurable AI meta-surfaces: An idea whose time has come," *EURASIP Jour. Wireless Communic. and Netw.*, vol. 2019, no. 1, pp. 1–20, 2019.

[2] E. Basar *et al.*, "Wireless communications through reconfigurable intelligent surfaces," *IEEE Access*, vol. 7, pp. 116 753–116 773, 2019.

[3] E. Calvanese Strinati *et al.*, "Wireless environment as a service enabled by reconfigurable intelligent surfaces: The RISE-6G perspective," *Proc. of EuCNC/6G Summit*, pp. 562–567, 2021.

[4] E. Calvanese Strinati, G. C. Alexandropoulos *et al.*, "Reconfigurable, intelligent, and sustainable wireless environments for 6G smart connectivity," *IEEE Communic. Mag.*, vol. 59, no. 10, pp. 99–105, 2021.

[5] C. Huang, A. Zappone, G. C. Alexandropoulos, M. Debbah, and C. Yuen, "Reconfigurable intelligent surfaces for energy efficiency in wireless communication," *IEEE Trans. Wireless Communic.*, vol. 18, no. 8, pp. 4157–4170, 2019.

[6] R. Xiong, X. Dong, T. Mi, and R. C. Qiu, "Optimal discrete beamforming of reconfigurable intelligent surface," *arXiv preprint arXiv:2211.04167*, 2022.

[7] P. Di Lorenzo, M. Merluzzi, E. Calvanese Strinati, and S. Barbarossa, "Dynamic edge computing empowered by reconfigurable intelligent surfaces," *EURASIP Jour. on Wireless Comm. and Netw.*, no. 1, 2022.

[8] C. L. Nguyen, O. Georgiou, and G. Gradoni, "Reconfigurable intelligent surfaces and machine learning for wireless fingerprinting localization," *arXiv preprint arXiv:2010.03251*, 2020.

[9] H. Wymeersch, J. He, B. Denis, A. Clemente, and M. Juntti, "Radio localization and mapping with reconfigurable intelligent surfaces: Challenges, opportunities, and research directions," *IEEE Veh. Tech. Magaz.*, vol. 15, no. 4, pp. 52–61, 2020.

[10] G. C. Alexandropoulos, I. Vinieratou, and H. Wymeersch, "Localization via multiple reconfigurable intelligent surfaces equipped with single receive RF chains," *IEEE Wireless Communic. Letters*, vol. 11, no. 5, pp. 1072–1076, 2022.

[11] A. Elzanaty, A. Guerra, F. Guidi, and M.-S. Alouini, "Reconfigurable intelligent surfaces for localization: Position and orientation error bounds," *IEEE Trans. Signal Process.*, vol. 69, pp. 5386–5402, 2021.

[12] C. L. Nguyen, O. Georgiou, G. Gradoni, and M. Di Renzo, "Wireless fingerprinting localization in smart environments using reconfigurable intelligent surfaces," *IEEE Access*, vol. 9, pp. 135 526–135 541, 2021.

[13] H. Wymeersch and B. Denis, "Beyond 5G wireless localization with reconfigurable intelligent surfaces," in *ICC 2020 IEEE Inter. Conf. on Communic. (ICC)*, 2020, pp. 1–6.

[14] F. Ghaseminajm, M. Alsmadi, D. Tubail, and S. S. Ikki, "RIS-aided mobile localization error bounds under hardware impairments," *IEEE Trans. Communic.*, vol. 70, no. 12, pp. 8331–8341, 2022.

[15] Z. Zhang, L. Wu, J. Dang, B. Zhu, and L. Wang, "Multiple RSS fingerprint based indoor localization in RIS-assisted 5G wireless communication system," *The Inter. Archives of Photogr., Remote Sensing and Spatial Inform. Sciences*, vol. 46, pp. 287–292, 2022.

[16] S.-P. Kuo and Y.-C. Tseng, "Discriminant minimization search for large-scale RF-based localization systems," *IEEE Trans. Mobile Comput.*, vol. 10, no. 2, pp. 291–304, 2010.

[17] J. Krumm and J. Platt, "Minimizing calibration effort for an indoor 802.11 device location measurement system," *Micros. Res.*, p. 8, 2003.

[18] R. Levie, Ç. Yapar, G. Kutyniok, and G. Caire, "RadioUNet: Fast radio map estimation with convolutional neural networks," *IEEE Trans. Wireless Communic.*, vol. 20, no. 6, pp. 4001–4015, 2021.

[19] A. E. C. Redondi, "Radio map interpolation using graph signal processing," *IEEE Communic. Letters*, vol. 22, no. 1, pp. 153–156, 2017.

[20] P. Di Lorenzo, S. Barbarossa, and P. Banelli, "Sampling and recovery of graph signals," *in Cooperative and Graph Signal Processing: Principles and Applications, Elsevier*, 2018.

[21] S. Barbarossa and S. Sardellitti, "Topological signal processing over simplicial complexes," *IEEE Trans. Signal Process.*, vol. 68, pp. 2992–3007, Mar. 2020.

Authorized licensed use limited to: Universita degli Studi di Roma La Sapienza. Downloaded on May 07,2024 at 07:34:19 UTC from IEEE Xplore. Restrictions apply.
© 2024 IEEE. Personal use is permitted, but republication/redistribution requires IEEE permission. See https://www.ieee.org/publications/rights/index.html for more information.